

Determination of the beam asymmetry Σ in η - and η' -photoproduction using Bayesian statistics

JAKOB MICHAEL KRAUSE

Masterarbeit in Physik
angefertigt im Helmholtz-Institut für Strahlen- und
Kernphysik

vorgelegt der
Mathematisch-Naturwissenschaftlichen Fakultät
der
Rheinischen Friedrich-Wilhelms-Universität
Bonn

Sep 2022

DRAFT

I hereby declare that this thesis was formulated by myself and that no sources or tools other than those cited were used.

Bonn,
Date

.....
Signature

- 1. Gutachterin: JUN. PROF. DR. ANNIKA THIEL
- 2. Gutachter: PROF. DR. JOCHEN DINGFELDER

DRAFT

Contents

1	Introduction	1
1.1	Photoproduction of Pseudoscalar Mesons	4
1.2	Measurement of Polarization Observables	5
1.3	Introduction to BAYESIAN statistics	5
1.3.1	Frequentist Approach	5
1.3.2	Bayesian approach	5
1.3.3	Combining inferences	5
1.4	Motivation and Structure of this Thesis	5
2	Experimental Setup	7
2.1	Production of (polarized) high energy photon beam	7
2.1.1	Tagger	8
2.2	Beam Target	8
2.3	Calorimeters	8
2.4	Trigger	8
3	Event selection	11
3.1	Reconstruction of events	12
3.2	Preselection and charge cut	12
3.3	Time of particles	13
3.4	Kinematic constraints	15
3.4.1	Derivation of cut conditions	15
3.4.2	Determination of cut ranges	16
3.4.3	Quality of event selection	21
3.5	Investigation of background and additional cuts	23
3.5.1	Inspecting plausibility of background reactions	23
3.5.2	Misidentification of background reactions	26
3.5.3	Examination of additional cuts	31
3.6	Summary of event selection	34
3.6.1	Reaction $\gamma p \rightarrow p\eta' \rightarrow p\gamma\gamma$	34
3.6.2	Reaction $\gamma p \rightarrow p\eta \rightarrow p\gamma\gamma$	35
4	Extraction of the beam asymmetries Σ_η and $\Sigma_{\eta'}$	37
4.1	Methods	38
4.1.1	Event yield asymmetries	38
4.1.2	Event based fit	41

4.2	Determination of Σ_{η} using Bayesian statistics	44
4.2.1	Application of methods to toy Monte Carlo data	44
4.2.2	Application of methods to data	53
4.2.3	Discussion	56
4.3	Determination of $\Sigma_{\eta'}$	58
4.3.1	Application of event based fit to toy Monte Carlo data	58
4.3.2	Application of event based fit to data	64
4.3.3	Systematic error	68
5	Discussion	73
5.1	Comparison of results to existing data	73
5.2	Comparison of results to PWA calculations	75
5.3	Final discussion of methods	77
6	Summary and outlook	79
A	Additional plots and calculations	81
A.1	Statistical error for the asymmetry $A(\phi)$	81
A.2	Kinematic variables for each bin	83
A.2.1	Coplanarity	83
A.2.2	Polar angle difference	85
A.2.3	Missing mass	87
A.2.4	Invariant mass	89
B	Discussion of binned fits	91
C	Investigation of posteriors without truncation	93
	Bibliography	97
	List of Figures	101
	List of Tables	107

Experimental Setup

As motivated in the previous chapter, it is promising to study the photoproduction of pseudoscalar mesons in order to determine a complete set of polarization observables. This requires a polarized photon beam and/or a polarized target. It is convenient to study photoproduction off a fixed target and investigate the resonances that occur in the process. Incidentally, these resonances can only be accessed via their decay products, such that suitable calorimeters are needed. The CBELSA/TAPS experiment is located in Bonn at the ELectron Stretcher Accelerator (ELSA), which can be used to generate a high energy photon beam using the *bremsstrahlung* process, meets all above mentioned requirements. This chapter will elaborate on the already mentioned parts of the experiment that was used to collect the data needed for the determination of the target asymmetry in η' photoproduction.

2.1 Production of (polarized) high energy photon beam

First of all, a high energy photon beam has to be produced.

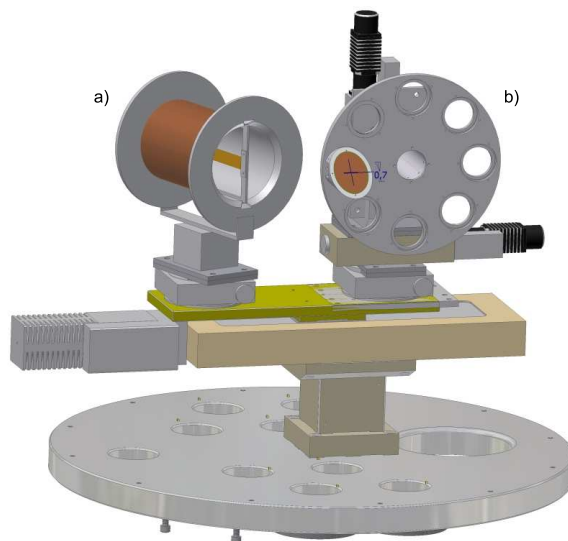


Figure 2.1: [Wal]

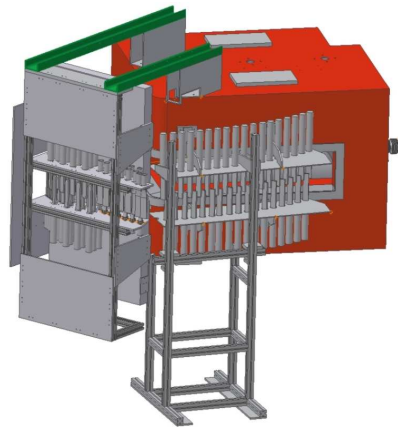


Figure 2.2: [Wal]

2.1.1 Tagger

2.2 Beam Target



Figure 2.3: [Wal]

2.3 Calorimeters

2.4 Trigger

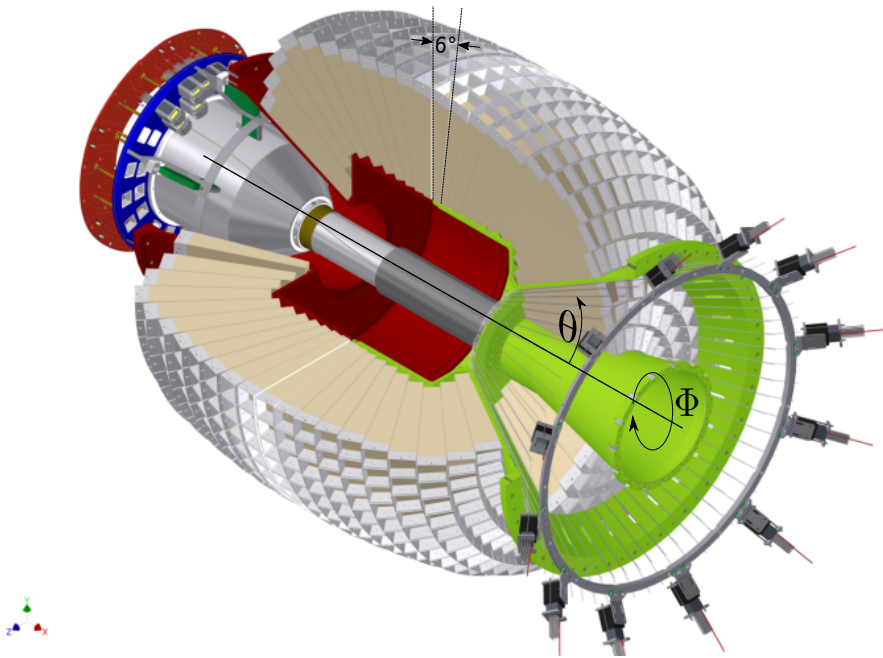


Figure 2.4: D. WALTHER in [Urb17]

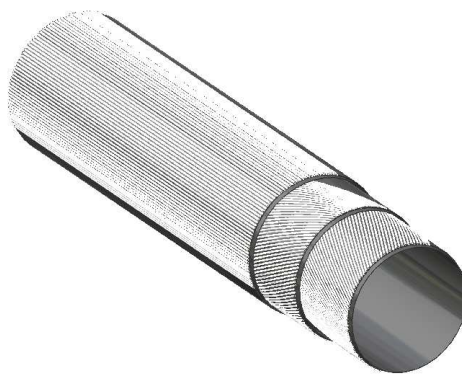


Figure 2.5: [Wal]

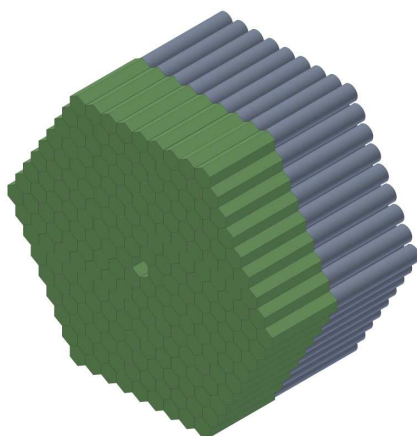


Figure 2.6: [Wal]

Bibliography

- [Wor+22] R. L. Workman et al., *Review of Particle Physics*, PTEP **2022** (2022) 083C01 (cit. on pp. 2, 3, 11–13, 16, 18, 26, 73, 75).
- [LMP01] U. Löring, B. Metsch and H. Petry, *The light-baryon spectrum in a relativistic quark model with instanton-induced quark forces*, The European Physical Journal A **10** (2001) 395, ISSN: 1434-601X, URL: <http://dx.doi.org/10.1007/s100500170105> (cit. on pp. 2, 3).
- [KS03] B. Krusche and S. Schadmand, *Study of nonstrange baryon resonances with meson photoproduction*, Prog. Part. Nucl. Phys. **51** (2003) 399, arXiv: nucl-ex/0306023 (cit. on pp. 3, 4).
- [Afz19] F. N. Afzal, *Measurement of the beam and helicity asymmetries in the reactions $\gamma p \rightarrow p\pi^0$ and $\gamma p \rightarrow p\eta$* , PhD thesis: Rheinische Friedrich-Wilhelms-Universität Bonn, 2019, URL: <https://hdl.handle.net/20.500.11811/8064> (cit. on pp. 4, 11, 21, 23, 35, 36, 38, 39, 43, 44, 48, 49, 53, 56, 59, 60, 68, 70, 73, 77).
- [DT92] D. Drechsel and L. Tiator, *Threshold pion photoproduction on nucleons*, J. Phys. G **18** (1992) 449 (cit. on p. 4).
- [Bar+18] M. Bartelmann et al., *Theoretische Physik 3 — Quantenmechanik*, 2018, ISBN: 978-3-662-56071-6 (cit. on p. 4).
- [Bar89] R. J. Barlow, *Statistics, A Guide to the Use of Statistical Methods in the Physical Sciences*, Wiley, 1989 (cit. on pp. 5, 39, 40, 45).
- [Wal] D. Walther, *Crystal Barrel, A 4 π photon spectrometer*, URL: <https://www.cb.uni-bonn.de> (visited on 27/09/2021) (cit. on pp. 7–10).
- [Urb17] M. Urban, *Design eines neuen Lichtpulsersystems sowie Aufbau und Inbetriebnahme der neuen APD Auslese für das Crystal-Barrel-Kalorimeter*, PhD thesis: Rheinische Friedrich-Wilhelms-Universität Bonn, 2017 (cit. on pp. 9, 12).
- [Afz12] F. N. Afzal, *Analysis of Crystal Barrel Data - Measurement of the double polarization observable E in the reaction $\vec{\gamma}\vec{p} \rightarrow \eta' p$* , Master thesis: Rheinische Friedrich-Wilhelms-Universität Bonn, 2012 (cit. on p. 11).
- [Dah08] T. Dahlke, *Bestimmung einer winkelabhängigen Energiekorrekturfunktion für das TAPS-Kalorimeter des Crystal-Barrel/TAPS-Experiments and ELSA*, Diploma thesis: Rheinische Friedrich-Wilhelms-Universität Bonn, 2008 (cit. on p. 12).
- [GP08] M. Grüner and D.-M. Piontek, *Hit reconstruction in ChaPI*, CB-TR16 Note 003 (2008) (cit. on p. 12).

- [Ike+00] H. Ikeda et al., *A detailed test of the CsI(Tl) calorimeter for BELLE with photon beams of energy between 20-MeV and 5.4-GeV*, Nucl. Instrum. Meth. A **441** (2000) 401 (cit. on pp. 18, 20).
- [Cre+09] V. Crede et al., *Photoproduction of eta and eta-prime mesons off protons*, Phys. Rev. C **80** (2009) 055202, arXiv: 0909.1248 [nucl-ex] (cit. on pp. 18, 23, 26).
- [Har17] J. Hartmann, *Measurement of Double Polarization Observables in the Reactions $\gamma p \rightarrow p\pi^0$ and $\gamma p \rightarrow p\eta$ with the Crystal Barrel/TAPS Experiment at ELSA*, Rheinische Friedrich-Wilhelms-Universität Bonn, 2017, URL: <https://hdl.handle.net/20.500.11811/7258> (cit. on pp. 23, 41, 43).
- [Die+20] M. Dieterle et al., *Helicity-Dependent Cross Sections for the Photoproduction of π^0 Pairs from Nucleons*, Physical Review Letters **125** (2020), URL: <https://doi.org/10.1103/PhysRevLett.125.062001> (cit. on p. 26).
- [Käs+18] A. Käser et al., *First measurement of helicity-dependent cross sections in $\pi^0\eta$ photoproduction from quasi-free nucleons*, Physics Letters B **786** (2018) 305, URL: <https://doi.org/10.1016/j.physletb.2018.10.006> (cit. on p. 26).
- [Bar+05] O. Bartholomy et al., *Neutral-Pion Photoproduction off Protons in the Energy Range $0.3 \text{ GeV} < E_\gamma < 3 \text{ GeV}$* , Physical Review Letters **94** (2005), URL: <https://doi.org/10.1103/PhysRevLett.94.012003> (cit. on p. 26).
- [Sta+11] A. Starostin et al., *Measurement of $3\pi^0$ photoproduction on the proton from threshold to 1.4 GeV*, 2011, URL: <https://arxiv.org/abs/1101.3744> (cit. on p. 26).
- [Mur+20] N. Muramatsu et al., *Differential cross sections, photon beam asymmetries, and spin density matrix elements of ω photoproduction off the proton at $E_\gamma = 1.3 - 2.4 \text{ GeV}$* , Phys. Rev. C **102** (2 2020) 025201, URL: <https://link.aps.org/doi/10.1103/PhysRevC.102.025201> (cit. on p. 26).
- [Str+76] W. Struczinski et al., *Study of photoproduction on hydrogen in a streamer chamber with tagged photons for $1.6 \text{ GeV} < E_\gamma < 6.3 \text{ GeV}$ Topological and reaction cross sections*, Nuclear Physics B **108** (1976) 45, ISSN: 0550-3213, URL: <https://www.sciencedirect.com/science/article/pii/0550321376901231> (cit. on p. 26).
- [Dug+09] M. Dugger et al., *π^+ photoproduction on the proton for photon energies from 0.725 to 2.875 GeV*, Physical Review C **79** (2009), URL: <https://doi.org/10.1103/PhysRevC.79.065206> (cit. on p. 26).
- [Mah22] P. Mahlberg, *Thesis in Preparation*, Rheinische Friedrich-Wilhelms-Universität Bonn, 2022 (cit. on pp. 34, 66, 68).

-
- [San+11] A. M. Sandorfi, S. Hoblit, H. Kamano and T.-S. H. Lee, *Determining pseudoscalar meson photoproduction amplitudes from complete experiments*, Journal of Physics G: Nuclear and Particle Physics **38** (2011) 053001, ISSN: 1361-6471, URL: <http://dx.doi.org/10.1088/0954-3899/38/5/053001> (cit. on p. 37).
- [Afz+20] F. Afzal et al., *Observation of the $p\eta'$ Cusp in the New Precise Beam Asymmetry Σ Data for $\gamma p \rightarrow p\eta$* , Phys. Rev. Lett. **125** (15 2020) 152002, URL: <https://link.aps.org/doi/10.1103/PhysRevLett.125.152002> (cit. on pp. 38, 77).
- [Pov+14] B. Povh, K. Rith, C. Scholz, F. Zetsche and W. Rodejohann, *Teilchen und Kerne, Eine Einführung in die physikalischen Konzepte*, vol. 9, Springer Spektrum, 2014 (cit. on p. 39).
- [RP22] G. van Rossum and the Python development team, *The Python Language Reference, Release 3.10.5, 2022*, URL: <https://docs.python.org/3.10/reference/index.html> (cit. on pp. 40, 56).
- [Vir+20] P. Virtanen et al., *SciPy 1.0: Fundamental Algorithms for Scientific Computing in Python*, Nature Methods **17** (2020) 261 (cit. on p. 40).
- [BR97] R. Brun and F. Rademakers, *ROOT — An object oriented data analysis framework*, Nucl. Instrum. Meth. A **389** (1997) 81, ISSN: 0168-9002, URL: <https://www.sciencedirect.com/science/article/pii/S016890029700048X> (cit. on pp. 40, 43, 44, 56).
- [sci] scipy, *scipy.optimize.curve_fit, Function Documentation*, URL: https://docs.scipy.org/doc/scipy/reference/generated/scipy.optimize.curve_fit.html (visited on 28/06/2022) (cit. on p. 40).
- [ROOa] ROOT, *TH1 Class reference*, URL: <https://root.cern.ch/doc/master/classTH1.html#a63eb028df86bc86c8e20c989eb23fb2a> (visited on 28/06/2022) (cit. on p. 40).
- [Gel+14] A. Gelman et al., *Bayesian Data Analysis*, vol. 3, Chapman & Hall/CRC, 2014 (cit. on p. 40).
- [Sta22a] Stan development team, *Prior Choice Recommendations*, 2022, URL: <https://github.com/stan-dev/stan/wiki/Prior-Choice-Recommendations> (cit. on p. 40).
- [Sta22b] Stan development team, *Stan Modeling Language Users Guide and Reference Manual*, vol. 2.29, 2022, URL: <https://mc-stan.org> (cit. on pp. 40, 43, 56, 61, 64, 77).
- [HG14] M. D. Hoffman and A. Gelman, *The No-U-Turn Sampler: Adaptively Setting Path Lengths in Hamiltonian Monte Carlo*, Journal of Machine Learning Research **15** (2014) 1593, URL: <http://jmlr.org/papers/v15/hoffman14a.html> (cit. on pp. 40, 43).

- [ROOb] ROOT, *TTree Class reference*,
URL: <https://root.cern.ch/doc/master/classTTree.html#a3e6bf252ab8653b47cc9116950f3ee7b> (visited on 28/06/2022) (cit. on p. 43).
- [JR75] F. James and M. Roos, *Minuit - a system for function minimization and analysis of the parameter errors and correlations*, Computer Physics Communications **10** (1975) 343, ISSN: 0010-4655, URL: <https://www.sciencedirect.com/science/article/pii/0010465575900399> (cit. on p. 43).
- [ROOc] ROOT, *TF1 Class reference*, URL: <https://root.cern.ch/doc/master/classTF1.html#a410b0219e18e80d3e305b4d97374c077> (visited on 28/06/2022) (cit. on p. 44).
- [Veh+19] A. Vehtari, A. Gelman, D. Simpson, B. Carpenter and P.-C. Bürkner, *Rank-normalization, folding, and localization: An improved \widehat{R} for assessing convergence of MCMC*, arXiv e-prints, arXiv:1903.08008 (2019) arXiv:1903.08008, arXiv: 1903.08008 [stat.CO] (cit. on p. 48).
- [Leo94] W. R. Leo, *Techniques for Nuclear and Particle Physics Experiments, A How-to Approach*, vol. 2, Springer-Verlag Berlin Heidelberg GmbH, 1994 (cit. on p. 73).
- [Lev+14] P. Levi Sandri et al., *First Measurement of the Σ Beam Asymmetry in η' Photoproduction off the Proton near Threshold*, (2014) (cit. on pp. 73, 75).
- [Col+17] P. Collins et al., *Photon beam asymmetry Σ for η and η' photoproduction from the proton*, Physics Letters B (2017) (cit. on pp. 73–75).
- [Tia+18] L. Tiator et al., *Eta and etaprime photoproduction on the nucleon with the isobar model EtaMAID2018*, The European Physical Journal A **54** (2018), URL: <https://doi.org/10.1140/epja/i2018-12643-x> (cit. on pp. 75, 76).

List of Figures

1.1	Running coupling of QCD. The colored data points represent different methods to obtain a value for α_s . For more details it may be referred to [Wor+22].	2
1.2	Calculated nucleon (isospin $I = 1/2$) resonances compared to measurements. Left in each column are the calculations [LMP01], the middle shows the measurements and PDG rating [Wor+22]	3
1.3	FEYNMAN diagram for the s-channel photoproduction of pseudoscalar mesons, adapted from [Afz19]	4
2.1	[Wal]	7
2.2	[Wal]	8
2.3	[Wal]	8
2.4	D. WALTHER in [Urb17]	9
2.5	[Wal]	9
2.6	[Wal]	10
3.1	Distribution of event classes in $\eta' \rightarrow \gamma\gamma$ production	13
3.2	Time information of all final state particles and the beam photon for 3PED η' production	14
3.3	Reaction time t_r for 3PED and 2.5PED η' production. The yellow region indicate the sidebands while the purple colored interval is the selected prompt peak.	15
3.4	Coplanarity of the $p\eta'$ final state with all other cuts applied for the energy bin $1500 \text{ MeV} \leq E_\gamma < 1600 \text{ MeV}$. The vertical dashed lines show the cut ranges obtained from a gaussian fit to the data (open circles). The solid black histograms represent fitted MC data of $\eta' \rightarrow \gamma\gamma$	19
3.5	Polar angle difference of the $p\eta'$ final state with all other cuts applied for the energy bin $1500 \text{ MeV} \leq E_\gamma < 1600 \text{ MeV}$. The vertical dashed lines show the cut ranges obtained from a gaussian fit to the data (open circles). The solid black histograms represent fitted MC data of $\eta' \rightarrow \gamma\gamma$	20
3.6	Missing mass of the $p\eta'$ final state with all other cuts applied for the energy bin $1500 \text{ MeV} \leq E_\gamma < 1600 \text{ MeV}$. The vertical dashed lines show the cut ranges obtained from a fit to data (open circles) employing a Novosibirsk function. The solid colored histograms represent fitted MC data from relevant photoproduction reactions: in black η' , in green π^0 , in red η , in blue ω , in yellow $2\pi^0$, magenta $\pi^0\eta$. The turquoise histogram is the sum of all MC histograms.	21

3.7	Invariant mass of the $p\eta'$ final state with all other cuts applied for all energy and angular bins. The open circles represent the measured data, the solid colored histograms fitted MC data from relevant photoproduction reactions: in black η' , in green π^0 , in red η , in blue ω , in yellow $2\pi^0$ and in magenta $\pi^0\eta$. The turquoise histogram is the sum of all MC histograms.	22
3.8	Invariant mass of the $p\eta'$ final state with all other cuts applied for the energy bin $1500 \text{ MeV} \leq E_\gamma < 1600 \text{ MeV}$. The vertical dashed lines show the cut ranges obtained from a gaussian fit to the η' MC data (solid black histogram). The open circles represent the measured data, the solid colored histograms fitted MC data from relevant photoproduction reactions: in black η' , in green π^0 , in red η , in blue ω , in yellow $2\pi^0$ and in magenta $\pi^0\eta$. The turquoise histogram is the sum of all MC histograms. . . .	22
3.9	Acceptance for the reaction $\gamma p \rightarrow p\eta'$ after all cuts that have been discussed so far for 2.5PED and 3PED events	23
3.10	Fraction of background events in the analyzed beam energy and angular bins.	24
3.11	Acceptance for possible background contributions	25
3.12	Generated energies of γ_3 and γ_4 in $2\pi^0$ and $\pi^0\eta$ photoproduction MC data. The threshold of 20 MeV is marked by a vertical red line. E_{γ_4} is shown on the top, E_{γ_3} is shown on the bottom of each figure.	27
3.13	E_γ^{gen} vs. E_γ^{rec} of γ_1 and γ_2 for $2\pi^0$ (top) and $\pi^0\eta$ (bottom) production. The slope $E_\gamma^{\text{gen}} = E_\gamma^{\text{rec}}$ is marked by a solid line.	29
3.14	Polar angle difference $\Delta\theta$ between γ_2 and γ_3 of the $\pi^0\eta$ final state.	30
3.15	Illustration of the misidentification process during reconstruction. Enumeration of photons is now arbitrary.	30
3.16	Generated CMS angle $\cos\theta_{\text{gen.}}$ vs. reconstructed CMS angle $\cos\theta_{\text{rec.}}$ for both background reactions. The slope $\cos\theta_{\text{gen.}} = \cos\theta_{\text{rec.}}$ is indicated by the solid line. . .	31
3.17	Detector hits of the recoil proton, as obtained from MC data for the production of η' , $2\pi^0$ and $\pi^0\eta$. CB: Crystal Barrel, FW: forward dector, MT: MiniTAPS	33
3.18	Difference in measured and calculated beam energy. Data points are shown as open circles, MC data as solid histograms: in black η' , in green π^0 , in red η , in blue ω , in yellow $2\pi^0$ and in magenta $\pi^0\eta$. The turquoise histogram is the sum of all MC histograms.	34
3.19	Invariant mass spectrum passing different stages in the event selection process. In the end clear peaks for all possibly produced mesons are visible. The vertical lines indicate the mean cut ranges over all energy and angle bins.	35
3.20	Invariant mass spectrum passing different stages in the event selection process. In the end clear peaks for all possibly produced mesons are visible. Taken from [Afz19]. . .	36
4.1	Left: Definition of angles α, ϕ, φ . Right: Photon momentum \vec{k} and polarization $\vec{\epsilon}$ define the beam polarization plane while the reaction plane is defined by the recoil proton p and produced meson M	37

-
- 4.2 Posterior predictive checks $p(A_{\text{rep}}|A)$ from a BAYESIAN fit to the event yield asymmetries for six toy Monte Carlo bins are shown as distributions. The data points in the upper plot are the asymmetry $A(\phi)$, which was additionally fitted using a χ^2 fit (solid line). The goodness of fit is shown using p -values, which give the fraction $T(A_{\text{rep}} > A)$ of replicated samples greater than the original measured value, with propagated statistical error bars on the bottom of each plot. The expected mean value of $T(A_{\text{rep}} > A) = 0.5$ is indicated by the dashed line. 46
- 4.3 p values of all toy Monte Carlo bins. They are centered around their mean at 0.5, which is indicated by the dashed line, and show no bias towards higher or lower values, thus confirming an adequate fit. 47
- 4.4 Left: Combined posterior distributions of all 10000 fits normalized by their respective standard deviation. Right: Unaltered combined posterior distributions of all 10000 fits. A GAUSSIAN fit was performed to determine mean μ and standard deviation σ of the distributions with results given on top. 47
- 4.5 Left: relative error $\frac{\sigma_{\text{MCSE}}}{\text{median}[p(\Sigma|y)]}$ Right: \hat{R} associated with the fit parameter Σ . Both are shown for all 10000 fits. The critical values that should not be exceeded are marked by dashed lines. 48
- 4.6 Combined posteriors for the beam asymmetries Σ and Σ^{bkg} from all 1000 event based fits. Left: Residuals Ξ Right: Unnormalized posterior distributions. A GAUSSIAN fit is performed on the distributions with results for mean μ and standard deviation σ on top. 50
- 4.7 Combined posterior probabilities using the *pooled likelihood* approach. Left: Signal beam asymmetry, Right: background beam asymmetry. Mean and standard deviation as obtained from a Gaussian fit are shown on top 51
- 4.8 Left: relative error $\frac{\sigma_{\text{MCSE}}}{\text{median}[p(\Sigma|y)]}$ Right: \hat{R} associated with the fit parameter Σ . Both are shown for all 1000 fits. The critical values that should not be exceeded are marked by dashed lines. 51
- 4.9 Posterior predictive check using the draws of the detector coefficients a and b . Points with error bars are the polarization weighted sum of event yields. The dashed line is the mean of the predictive values while the solid opaque lines are representative of one simulation draw $a^{(s)}, b^{(s)}$ 52
- 4.10 Posterior predictive checks $p(A_{\text{rep}}|A)$ from a BAYESIAN fit to the event yield asymmetries for all angular bins of the energy bin $1250 \text{ MeV} \leq E_\gamma < 1310 \text{ MeV}$. The data points in the upper plot are the asymmetry $A(\phi)$, which was additionally fitted using a χ^2 fit (solid line). The goodness of fit is shown using p -values, which give the fraction $T(A_{\text{rep}} > A)$ of replicated samples greater than the original measured value, with propagated statistical error bars on the bottom of each plot. The expected mean value of $T(A_{\text{rep}} > A) = 0.5$ is indicated by the dashed line. 54
- 4.11 p values generated using all fits. They are centered around their mean at 0.5, which is indicated by the dashed line, and show no bias towards higher or lower values, thus confirming an adequate fit. 55
- 4.12 Left: relative error $\frac{\sigma_{\text{MCSE}}}{\text{median}[p(\Sigma|y)]}$ Right: \hat{R} associated with the fit parameter Σ . Both are shown for all $11 \cdot 12$ binned fits to the asymmetry $A(\phi)$. The critical values that should not be exceeded are marked by dashed lines. 55

4.13	Left: relative error $\frac{\sigma_{\text{MCSE}}}{\text{median}[p(\Sigma y)]}$ Right: \hat{R} associated with the fit parameter Σ . Both are shown for all $11 \cdot 12$ unbinned fits. The critical values that should not be exceeded are marked by dashed lines.	56
4.14	Posterior predictive check using the draws of the detector coefficients a and b for the kinematic bin $1250 \text{ MeV} \leq E_\gamma < 1310 \text{ MeV}, 0 \leq \cos \theta < 0.17$. Points with error bars are the polarization weighted sum of event yields. The dashed line is the mean of the predictive values while the solid opaque lines are representative of one simulation draw $a^{(s)}, b^{(s)}$	57
4.15	Final results for the beam asymmetry Σ in η photoproduction off the proton for all kinematic bins obtained with BAYESIAN methods. They are compared with the results of a least squares fit and an unbinned fit as given in reference [Afz19]. All results agree within statistical error bars or within the widths of marginal posterior distributions.	59
4.16	Normalized residuals (left) and unaltered distribution (right) of all 10000 fits for the beam asymmetry $\Sigma = (1 - \delta) \cdot \Sigma_1 + \delta \cdot \Sigma_2$. GAUSSIAN fits are performed with results given on top of each plot.	61
4.17	Normalized residuals (left) and unaltered distribution (right) of all 10000 fits for the background beam asymmetry Σ_t^{bkg} . GAUSSIAN fits are performed with results given on top of each plot.	62
4.18	Fitted efficiency function (red line) applied to the polarization weighted sum of event yields (data points) for one toy Monte Carlo bin. 12 bins in ϕ are built for demonstration.	62
4.19	Combined (added) posteriors of all 1000 fits. Left: Signal beam asymmetry Σ_1 Right: Background beam asymmetry Σ_t^{bkg} . A GAUSSIAN fit is performed with results given on top.	63
4.20	Combined (added) posteriors of all fits for the fit parameter Σ_2^{true} . A GAUSSIAN fit is performed which reproduces exactly the values that were used for the simulations.	64
4.21	MCMC diagnostics for the event based BAYESIAN fit. Left: MCSE, Right: \hat{R} -value. The critical values not to be exceeded are marked by the dashed lines.	65
4.22	Posterior predictive checks of one toy Monte Carlo bin using the draws from the marginal posteriors of the detector coefficients a, b (opaque blue lines). The mean values are marked by the dashed line and follow the distribution of the data points which are the polarization weighted sum of event yields, using 12 ϕ bins.	65
4.23	Final results for the beam asymmetry Σ in η' photoproduction. Two sets of results are shown: The dark blue distributions and orange data points with errorbars are obtained with an unbinned fit that does not consider any background contributions. The light blue distributions and data points are obtained with the modified BAYESIAN fit and by correcting the point estimates according to Equation (4.42), respectively. All errors are statistical errors only.	67
4.24	Results for the additionally fitted Σ_2^{true} (distributions) compared with the underlying data points [Mah22] with statistical errors. The error bars on average cover 1σ of the distributions, indicating a successful fit. All errors are statistical errors only.	68
4.25	MCMC diagnostics for the event based BAYESIAN fit. Left: MCSE, Right: \hat{R} -value. The critical values not to be exceeded are marked by the dashed lines.	69

4.26	Posterior predictive checks of the kinematic bin $1700 \text{ MeV} \leq E_\gamma < 1800 \text{ MeV}$, $0.67 \leq \cos \theta < 1$ using the draws from the marginal posteriors of the detector coefficients a, b (opaque blue lines). The mean values are marked by the dashed line and follow the distribution of the data points which are the polarization weighted sum of event yields, using 12 ϕ bins.	69
4.27	Final results for the beam asymmetry $\Sigma_{\eta'}$ for all energy and angular bins. Only the corrected results from the unbinned maximum likelihood fit and distributions from the modified BAYESIAN fit are shown. The bottom of each plot indicates the systematic error as gray bars. It was determined as previously discussed.	71
5.1	Results for the beam asymmetry $\Sigma_{\eta'}$ (orange errorbars and distributions) compared with the results for the energy bins $E_\gamma = 1569 \text{ MeV}$, $E_\gamma = 1676 \text{ MeV}$, $E_\gamma = 1729 \text{ MeV}$ reported in reference [Col+17] (black errorbars). Systematical errors are shown as grey bars.	74
5.2	Results for the beam asymmetry $\Sigma_{\eta'}$ (orange errorbars and distributions) compared with PWA solutions: etaMAID [Tia+18](dashed black line),. . . The errorbars only depict statistical error, the systematic error is shown as grey bars.	76
A.1	Coplanarity $\Delta\phi$ for all energy and angular bins. Data points are displayed as open circles, scaled Monte Carlo data belonging to η' photoproduction is displayed as solid histogram. The determined cut ranges are indicated by the dashed red lines.	83
A.1	Coplanarity $\Delta\phi$ for all energy and angular bins. Data points are displayed as open circles, scaled Monte Carlo data belonging to η' photoproduction is displayed as solid histogram. The determined cut ranges are indicated by the dashed red lines.	84
A.2	Polar angle difference $\Delta\theta$ for all energy and angular bins. Data points are displayed as open circles, scaled Monte Carlo data belonging to η' photoproduction is displayed as solid histogram. The determined cut ranges are indicated by the dashed red lines.	85
A.2	Polar angle difference $\Delta\theta$ for all energy and angular bins. Data points are displayed as open circles, scaled Monte Carlo data belonging to η' photoproduction is displayed as solid histogram. The determined cut ranges are indicated by the dashed red lines.	86
A.3	Missing mass m_x for all energy and angular bins. Data points are displayed as open circles, scaled Monte Carlo data belonging to η' (black), $2\pi^0$ (yellow) and $\pi^0\eta$ (magenta) photoproduction is displayed as solid histogram while their sum is displayed as turquoise histogram. The determined cut ranges are indicated by the dashed red lines.	87
A.3	Missing mass m_X for all energy and angular bins. Data points are displayed as open circles, scaled Monte Carlo data belonging to η' (black), $2\pi^0$ (yellow) and $\pi^0\eta$ (magenta) photoproduction is displayed as solid histogram while their sum is displayed as turquoise histogram. The determined cut ranges are indicated by the dashed red lines.	88
A.4	Invariant mass m_{meson} for all energy and angular bins. Data points are displayed as open circles, scaled Monte Carlo data belonging to η' (black), $2\pi^0$ (yellow), $\pi^0\eta$ (magenta), π^0 (green) and ω (blue) photoproduction is displayed as solid histogram while their sum is displayed as turquoise histogram. The determined cut ranges are indicated by the dashed red lines.	89

- A.4 Invariant mass m_{meson} for all energy and angular bins. Data points are displayed as open circles, scaled Monte Carlo data belonging to η' (black), $2\pi^0$ (yellow), $\pi^0\eta$ (magenta), π^0 (green) and ω (blue) photoproduction is displayed as solid histogram while their sum is displayed as turquoise histogram. The determined cut ranges are indicated by the dashed red lines. 90
- B.1 Fit performance in dependence of the number of bins. Left axis shows the mean μ of the distribution of the normalized residuals ξ , right axis shows the mean χ^2 of all fits. Squares simulate fits with statistics similar to the $\gamma p \rightarrow p\eta' \rightarrow p\gamma\gamma$ final state, triangles statistics similar to the $\gamma p \rightarrow p\eta \rightarrow p\gamma\gamma$ and final state, pentagons statistics similar to the $\gamma p \rightarrow p\pi^0 \rightarrow p\gamma\gamma$. Dotted red line indicates the ideal value of $\chi^2 = 1$, while the dashed blue line indicates the ideal mean of the normalized residuals at $\mu = 0$. 92
- C.1 Combined posteriors of all 1000 fits without truncation for the signal beam asymmetry Σ_1 and the background beam asymmetry Σ_t . Left: normalized residuals Ξ , Right: unaltered added posterior distributions. GAUSSIAN fits have been performed with results given on top of each plot. 94
- C.2 Posterior distributions of Σ_1 (left) and Σ_t (right) combined in an independent likelihood pool. GAUSSIAN fits to the distribution confirm the reproduction of the input values within 1σ . Note that only very few datapoints were available for the fits, because the distributions overwhelmingly converge into a single bin at ± 0.5 , hence the large errors on the fit parameters. 95

List of Tables

1.1	Summary of the particles of the SM	1
1.2	Allowed quantum numbers for the intermediate resonance state N^*/Δ^*	4
3.1	The five most probable decay modes of the η and η' meson. The most probable further decay with according branching ratio is shown in brackets.[Wor+22]	11
3.2	Examined MC reactions that were used in sum for the fit	17
3.3	Fit functions and cut ranges for each kinematic variable	18
3.4	Total cross sections σ in the energy range 1500 to 1800 MeV, branching ratios (BR) to $n\gamma$ final states, maximum acceptance \tilde{A} for signal and possible background contributions as well as the expected signal to background ratio R . References [Die+20] and [Käs+18] give the cross sections only up to roughly 1500 MeV, the given values are thus upper bounds. For the same reason, from reference [Sta+11] only a lower bound can be estimated. For all other reactions a rough mean over the energy bins of interest is built. If the references provide only differential cross sections a crude integration in each angular bin is performed. In case only very few ($O(10^1)$) decays pass event selection, the acceptance is built in one global bin only for the respective reactions. This is indicated by the horizontal line.	26
3.5	Relative loss in signal and background events if a cut on ΔE is applied.	32
4.1	Summary of the complete setting of all toy Monte Carlo experiments for the event based fit. Values and table layout adapted from [Afz19].	49
4.2	Summary of the complete setting of all toy Monte Carlo experiments for the event based fit. Table layout adapted from [Afz19].	60